Available online at www.sciencedirect.com
SCIENCE DIRECT®

Journal of the European Ceramic Society 23 (2003) 3021–3034
www.elsevier.com/locate/jeurceramsoc

Ordering and quality factor in $0.95BaZn_{1/3}Ta_{2/3}O_3$–$0.05SrGa_{1/2}Ta_{1/2}O_3$ production resonators

I.M. Reaney[a,*], P.L. Wise[a], I. Qazi[a], C.A. Miller[a], T.J. Price[b], D.S. Cannell[b], D.M. Iddles[b], M.J. Rosseinsky[c], S.M. Moussa[c], M. Bieringer[c], L.D. Noailles[c], R.M. Ibberson[d]

[a]*Department of Engineering Materials, University of Sheffield, Sheffield S1 3JD, UK*
[b]*Filtronic Comtek, Ceramics Division, Enterprise Drive, Four Ashes, Wolverhampton WV10 7DB, UK*
[c]*Department of Chemistry, University of Liverpool, Liverpool L69 7ZD, UK*
[d]*ISIS Facility, CLRC- Rutherford Appleton Laboratory, Chilton, Didcot, Oxon OX11 0QX, UK*

Received 15 August 2002; received in revised form 14 February 2003; accepted 22 February 2003

Abstract

Ordering of the B-site cations in UMTS (universal mobile telecommunications systems) standard resonator pucks composed of perovskite structured, $0.95BaZn_{1/3}Ta_{2/3}O_3$–$0.05SrGa_{1/2}Ta_{1/2}O_3$ (BZT–SGT) has been investigated using transmission electron microscopy (TEM), X-ray diffraction (XRD) and powder neutron diffraction (PND). XRD patterns from samples sintered at 1550 °C/2 h but annealed and quenched at 50 °C intervals between 1400 and 1600 °C revealed that the order–disorder phase transition was at ~1500 °C. In addition, a peak at ~29.5° 2θ attributed to a $Ba_8ZnTa_6O_{24}$ phase was present due to ZnO loss. Electron diffraction patterns revealed that samples heat treated ⩾1500 °C (including as sintered samples, 1525 °C/2h,) exhibited short-range 1:2 ordering along all <111> directions giving rise to an average short-range face centred cubic structure. Samples annealed and quenched from below 1500 °C showed 1:2 order. To avoid excessive ZnO loss, an annealing temperature was chosen at 1275 °C (for 24 and 168 h). Neutron diffraction data were best refined using two ordered BZT phases with slightly different lattice parameters. TEM revealed a microstructure in each case consisting of 1:2 small ordered domains in the centre of all grains but with every second grain exhibiting a concentric shell composed of an ordered single domain, containing elongated translational (APBs) but not orientational domains. The formation of the concentric ordered shell was attributed to grain boundary migration during grain growth. As-sintered samples gave unloaded quality factors (Q) = 54,000 at 2 GHz which rose to 78,000 at 2 GHz after annealing for 24 h. No further improvement in Q was observed for longer annealing times.

Keywords: $Ba(Zn,Ta)O_3$; Electron microscopy; Microwave dielectric properties; Neutron diffraction; Perovskites; $Sr(Ga,Ta)O_3$; X-ray diffraction

1. Introduction

Modified $Ba(Zn_{1/3}Ta_{2/3})O_3$ (BZT) is a microwave dielectric ceramic used in mobile phone base stations.[1] BZT doped with either 5 mol% $SrGa_{1/2}Ta_{1/2}O_3$ (SGT)[2] or 3–5 mol% $BaZrO_3$[3] has a temperature coefficient of the resonant frequency (τ_f) tunable through zero, a dielectric constant of 29 and a unloaded quality factor (Q) of 50–80,000 at a resonant frequency (f_o) of ~2 GHz (Q^*f_o = 100–150,000 GHz). BZT belongs to a class of compounds often referred to as 1:2 or 1/3:2/3 complex perovskites.[4] The structure of this phase is based on the simple cubic perovskite lattice in which corner shared, BO_6 octahedra describe a cuboctahedral A-site interstice.[4] However, the B-site cations are ordered in a 1:2 ratio on one set, for example (111) or $(\bar{1}\bar{1}\bar{1})$, of alternate pseudocubic {111} planes. The ordering sequence was initially described by Galasso[4] as the $Ba(Sr_{1/3}Ta_{2/3})O_3$ structure and is trigonal with a space group, P3m1.[5]

Many powder X-ray diffraction (XRD) studies have been performed on BZT and it has been known since the early 1980s that the degree of order increases on annealing typically between 1400 and 1600 °C.[5,6] This is accompanied by an increase in the microwave dielectric

* Corresponding author.
E-mail address: i.m.reaney@sheffield.ac.uk (I.M. Reaney).

0955-2219/03/$ - see front matter © 2003 Elsevier Ltd. All rights reserved.
doi:10.1016/S0955-2219(03)00117-1

quality factor, Q.[6] Ordering also gives rise to peak splitting of pseudocubic {111} peaks consistent with a trigonal space group and a distortion perpendicular to the pseudocubic {111} stacking planes.[4,6,7]

It was not until the late 1980s and 1990s that transmission electron microscopy (TEM) was used to investigate the degree of order in BZT,[7–9] revealing that ordered domains in BZT are typically about 10–30 nm in diameter and usually do not grow beyond these dimensions as time at temperature is increased.[7–9] There has been little postulation in the literature on this observation but the appearance of strain contrast at the domain boundaries[9] suggests that growth is inhibited by the trigonal distortion.

During the mid to late 1980s, several authors published TEM studies of ordering in other complex perovskites and the understanding of the order–disorder transition in some materials improved. 1:1 or 0.5:0.5 complex perovskites form an ordered rock salt, fcc structure with a space group, Fm $\bar{3}$ m. Randall et al.[10,11] and Harmer et al.[8] extensively investigated $Pb(Sc_{1/2}Ta_{1/2})O_3$ (PST) and observed large (0.1–1 μm diameter) domains after annealing at approximately 900–1000 °C for several hours. Large elongated antiphase domains ($\sim 0.1 \times 0.5$ μm) were particularly common at the grain boundaries where diffusion rates are higher due to a greater point defect density.[10,11] $BaMg_{1/3}Ta_{2/3}O_3$ (BMT) is also a 1:2 complex perovskite and has the same trigonal space group as BZT. However, BMT that has been furnace cooled and has not undergone subsequent heat treatment is fully ordered with domains up to 1 μm diameter.[8] It is used only in applications where cost is not an issue and a high Q ($Q^* f_o > 200{,}000$, $\varepsilon_r = 24$) is paramount, since the fabricaton of crack free 2–3 GHz resonators is extremely difficult.

Reaney et al.[9] reported that the order–disorder phase transition temperature was between 1600 and 1650 °C for pure BZT. Heat treatment at 1600 °C resulted in a core shell ordering arrangement with 50 nm order domains in the centre of grains and larger 0.5 μm regions at the grain periphery. Translational domains, otherwise known as antiphase domain boundaries (APBs), were observed between regions that had nucleated on the same set of {111} planes but out of phase and 71/109° (the permitted angles between pseudocubic <111> directions) orientational domain walls were present between regions that had nucleated in phase but on different sets of {111} planes. Domain walls with a mixed translational and orientational character are possible but were not reported by these authors.

To the authors knowledge there has been no attempt to find the temperature at which the order–disorder transition occurs in commercial modified BZT systems, where small quantities of dopant cations are introduced to accelerate the formation of high Q material. Here, we report on the ordering behaviour of commercial resonator pucks of 0.95BZT–0.05SGT first noted by Kageyama et al.[2] A series of quenching experiments are performed to ascertain the approximate temperature of the order–disorder phase transition. This information is used to guide annealing experiments in an attempt to improve Q by inducing a greater degree of order in the system. The structure and microstructure of the ordered and disordered phases are investigated using TEM and neutron and X-ray diffraction. This provides a comprehensive picture of the evolution of the structure over different length scales, both locally and in a highly spatially resolved manner from TEM and quantitatively probing the entire sample while averaging over longer distances in neutron diffraction. This allows identification of the key structural features controlling Q in commercial BZT-based systems.

2. Experimental procedure

2.1. Ceramic processing

Standard electronic grade purity raw materials (>99.5%) with a d_{50} of approx 1–3 μm were batched in lots of 100–200 kg. Measurement accuracy for the individual powders were maintained to 0.002 kg. The powders were transferred to an attrition mill and milled for approx 3 h with deionised water and YSZ media. Milling was complete after 3 h and the d_{50} of the mix was below 3 μm. After spray drying the powder was calcined in a 1000 l furnace for 10 h at 1250 °C. Post calcination, the powders were re-milled in the attrition mill until the d_{50} of the slip was below 5 μm. Binders at 2 wt.% were subsequently added and the slip spray dried. Spray dried particulates were pressed in a 37 mm diameter die at 70 MPa. Sintering was undertaken at 1525 °C for 2 h with consideration being given to minimise ZnO loss during this process. A cooling rate of 90 °C/h was employed to promote an ordered material. All ceramics had >97% of theoretical density as measured using the Archimedes water immersion technique.

2.2. Heat treatment

2.2.1. Quenching

Samples for the order–disorder study were prepared by sintering under normal conditions and cooling at a rate of 3 °C/min. Samples were subsequently heated on a ZrO_2 board in a muffle furnace (ramp rate 3 °C/min) between 1400 and 1600 °C and held at temperature for 16 h. The furnace door was opened at temperature and the samples removed and dropped into water.

Samples for electrical characterisation and electron microscopy were annealed in a muffle furnace at 1275 °C for 24 and 168 h ramp rate 3 °C/min up and down from temperature.

2.3. Characterisation

2.3.1. Structural and microstructural

Conventional X-ray diffraction was performed on powdered samples using a Philips X-ray diffractometer. X-ray patterns were recorded at 2θ values between 10 and 80° at a scanning rate of 2° 2θ/min using non-monochromated Cu K_α radiation.

High resolution X-ray powder diffraction data were collected using a Stoe Stadi P diffractometer in reflection geometry with Cu K_{α_1} radiation and a linear position sensitive detector. Samples were dispersed in ethanol on a zero-background holder. Rietveld analysis of the X-ray data was performed with the GSAS suite of programmes[12]

Neutron powder diffraction data (on the sample annealed at 1275 °C for 1 week and on two samples annealed at 1275 °C for 24 h) were collected on the high resolution powder diffractometer HRPD at the ISIS spallation neutron source, Rutherford Appleton Laboratory, Didcot, Oxfordshire. Full profile analysis using the Rietveld method was performed with in-house software based on the Cambridge Crystallography Subroutine Library (CCSL).

Larger fragments of the quenched samples were used to prepare TEM samples. Pieces, approximately 3 mm diameter, were mounted on a Gatan disc grinder stub using Crystalbond 'heat on/heat off' resin. The ceramic was ground flat on one side using the Gatan disc grinder, removed from the Gatan disc grinder stub and remounted with the flat side down. The sample was further ground to approximately 20 μm thick and a 3.05 mm Cu support ring with 800 μm circular hole was glued onto its surface using an epoxy resin. The sample was removed from the stub and excess Crystalbond cleaned off its surface using acetone. The samples were thinned in a Gatan Duo Mill ion beam thinner operating at an accelerating voltage of 6 kV and a combined gun current of 0.6 mA at an incidence angle of 15°. The samples were examined using a Jeol 3010 TEM operating at an accelerating voltage of 300 kV.

2.3.2. Electrical

Microwave measurements were performed using a silver plated aluminium cavity $> \sim 4$ times the diameter of the test resonator (this ensured an "isolated" but shielded resonator) and a Agilent vector network analyzer (8753ES) with range from 30 kHz to 6 GHz. Sintered samples were located at the centre of the cavity on a 99.5% alumina support, thus avoiding any influence from the metallic cavity walls. Microwave energy was coupled to the test piece using a single probe, measuring in reflectance. After calibration for the cables and cavity, the coupling was adjusted such that losses were lower than −30 dB. Q is approximated using the following equation:

$$Q = f_0/\mathrm{BW} \tag{1}$$

where f_o is the resonant frequency and BW is the bandwidth measured at 7 dB from the resonant peak minimum. Measurement of Q was at ambient temperature and the resonance mode measured was $TE_{01\delta}$. τ_f measurements were performed in the same aluminium cavity placed inside a Tenney temperature control cabinet. Resonant frequency measurements were taken at 60, 20 and −10 °C when the $TE_{01\delta}$ mode was stable. τ_f was calculated using the following equation:

$$\tau_f = (f_{60} - f_{-10})/(f_{20} \times 70) \tag{2}$$

3. Results and discussion

3.1. As-sintered BZT–SGT

Fig. 1 shows secondary electron SEM images and energy dispersive X-ray spectra obtained from the surface of as-sintered BZT–SGT. The images reveal (a) a general microstructure composed of parallel regions of (b) large (15 μm) and (c) (1 μm) small equiaxed grains, surrounding acicular precipitates. Similar images were obtained from samples annealed at 1275 °C/24 h and 1275 °C/168 h. Energy dispersive X-ray analysis from both small and large equiaxed grains (Fig. 1d) showed that they contain Ba, Ta and Zn whereas the acicular grains (Fig. 1e) were Zn deficient. Desu and O'Bryan[6] and Kawashima et al.[13] both observed ZnO loss from the surface of BZT-based ceramics when fired in air.

3.2. Order–disorder behaviour

Several authors[3,6,14] have reported that the properties of BZT based ceramics may be improved by annealing below the order–disorder phase transition, thereby ordering the Zn and Ta cations into the trigonal supercell. The phase transformation temperature of pure BZT has been determined to be between 1600 and 1650 °C.[9] Fig. 2 shows a series of XRD patterns obtained from samples of BZT–SGT, annealed for 16 h at 1400–1550 °C and quenched into water directly from the furnace. At 1450 °C, the sample exhibits superlattice reflections consistent with the presence of a trigonal supercell. The reflections persist until 1450 °C but at 1500 °C the peaks have an almost zero intensity. By 1550 °C, superlattice peaks are completely absent. It is concluded therefore that the order–disorder phase transition in BZT–SGT occurs at ~1500 °C.

Fig. 3 shows <110> zone axis electron diffraction patterns from samples quenched from 1450, 1500 and 1550 °C. At 1450 °C, discrete $\pm{}^1/_3\{hkl\}$ superlattice reflections are observed, arising from two variants of

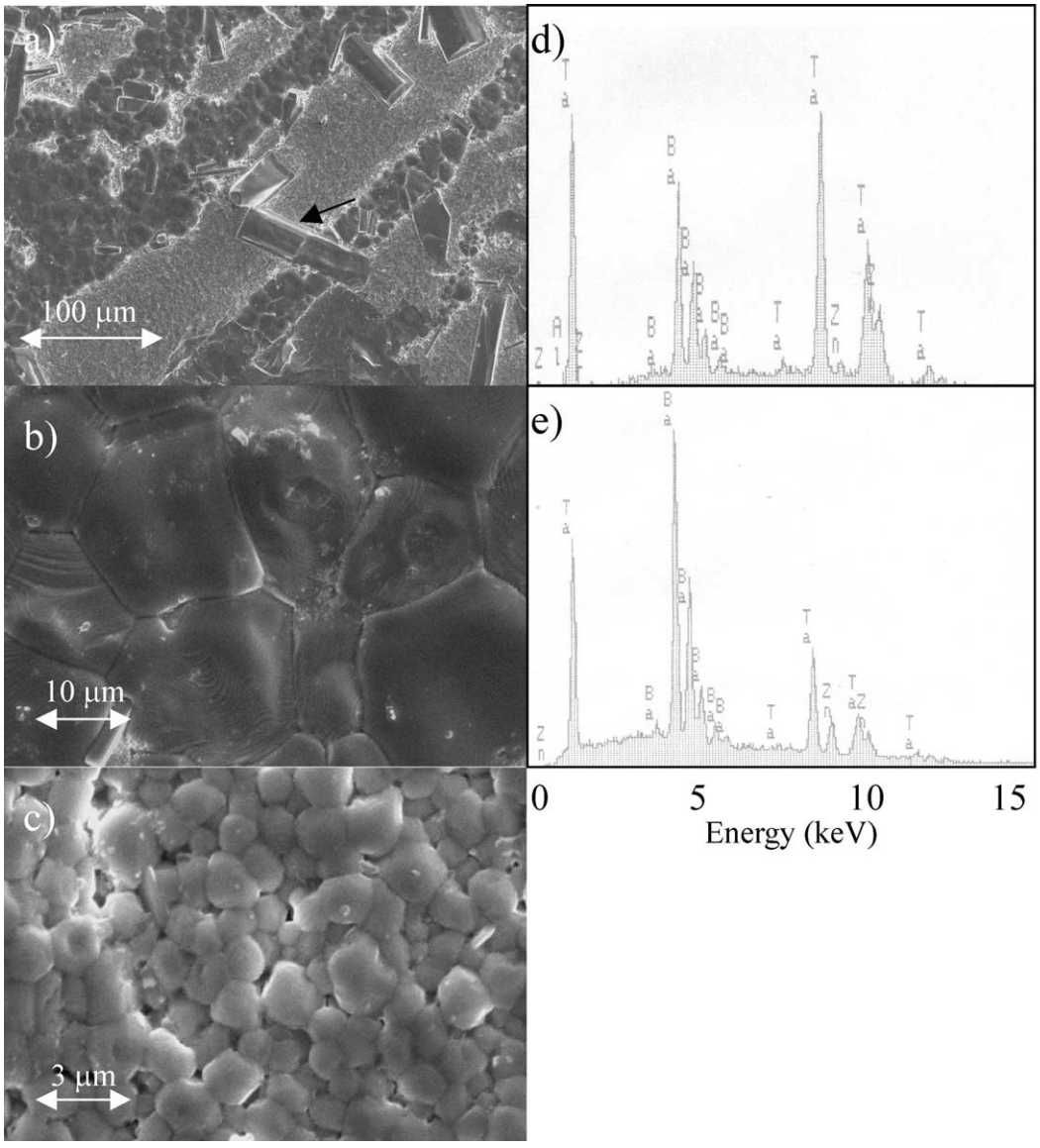

Fig. 1. Secondary electron SEM images EDS patterns obtained from the surface of as-sintered BZT–SGT showing (a) general area with acicular second phase (arrowed), (b) large equiaxed grain regions, (c) small equiaxed grain regions, (d) EDS pattern from second phase and (e) EDS pattern from small and large grains.

1:2 order, perpendicular to e.g. (111) and (11$\bar{1}$) planes. At 1500 °C and 1550 °C, only diffuse streaks of intensity parallel to e.g. [111] and [11−1] directions are observed. Above 1500 °C, local ordering is less than a coherent diffracting volume for electrons (1–2 nm) and may be considered as trigonal short range ordered. This gives rise to the streaking along pseudocubic <111> directions. The point of crossover of the streaks however, is at $^1/_2${hkl} positions, commonly associated with fcc rather than trigonal ordering.[9] The average structure therefore may also be viewed as short range fcc. Previous work[10] has associated these reflections with 1:1 ordering but the streaks coincide perfectly with $\pm^1/_3${hkl} positions for which the intensities at $^1/_2${hkl} positions (point of crossover) are approximately doubled. Davies et al [3] observed discrete 1:1 fcc ordered reflections in $(1-x)BaZn_{1/3}Ta_{2/3}O_3$–$xBaZrO_3$ (BZT-BZr) ceramics. 1:1 ordering in BZT-BZr however, is stabilised by charge compensation on the B-site, $(Zn^{2+} + {}^1/_4Zr^{4+})$:$Ta^{5+}$ and encouraged by the similar cation radii of Zn^{2+} and Zr^{4+} (~0.75 Å). In BZT–SGT, no such charge compensation and size matching occurs since Ga has a 3+ valence state and is smaller than Zn^{2+} (r_{Ga}≈0.61 Å). The intensity of the superlattice reflections from samples quenched from 1500 and 1550 °C were too low to obtain dark field images even under dynamical (two beam) conditions but at 1450 °C, discrete ordered regions ~10–20 nm diameter were observed, Fig. 4.

Table 1
Dependence of the dielectric properties and trigonal domain sizes of the BZT–SGT phase on thermal treatment

Sintering conditions	Annealing conditions	Area[a] (%)	Domain$_{(100)}$[b] (Å)	Domain[c]$_{(100)}$ (Å)	Domain[d] (Å)	Quality factor @2 GHz	ε_r	τ_f (ppm/°C)	f_0 (GHz)
1525 °C/2 h[c]	–	<1	<120			54,000	29	0	2
1525 °C/2 h	1275 °C/24 h	3.1(2), 3.3(2)	158(3), 183(8)	98(20), 126(23)		78,000	29	0	2
1525 °C/2 h	1275 °C/168 h	3.50(4)	290(6)	172(6)	100–200 (GC), 1000–2000 (GS)	77,000	29	0	2

The trigonal domain sizes of the ordered regions are as indicated by the FWHM of the (100) superstructure reflection of the $P\bar{3}m1$ ordered cell. The extent of order within the domains is qualitatively indicated by the area of the supercell reflection relative to the main perovskite subcell reflection at 31° 2θ.

[a] The area is of the (100) trigonal supercell reflection relative to the main intense peak at ~2θ 31&deg.

[b] The domain sizes were calculated using XRD data based on the FWHM of (100) reflection using the Scherrer equation. The instrumental contributions were accounted for by using standard Scheelite sample.

[c] Domain size calculated from NPD data.

[d] Domain sizes determined from TEM from Grain Core, GC, and Grain Shell, GS.

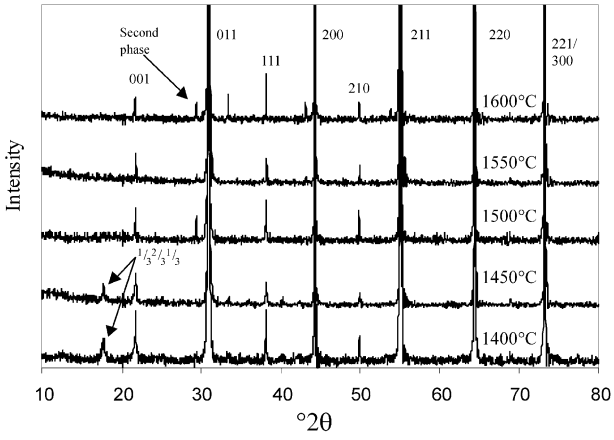

Fig. 2. XRD patterns obtained from samples of BZT–SGT, annealed for 16 h at 1400–1600 °C and quenched into water directly from the furnace. The 1600 °C pattern shows four reflections from the impurity phase at 29, 33, 43 and 54°.

3.3. Annealing studies and quality factors

Although dielectric property measurements cannot be performed on quenched samples, it is evident that ordering of Zn^{2+} and Ta^{5+} cations may be induced by annealing BZT–SGT below 1500 °C which according to Desu and O'Bryan,[6] Kawashima[14] and Davies et al.,[3] should improve Q. However, ZnO loss occurs in BZT based ceramics above 1300 °C.[6,13] Annealing in a ZnO rich atmosphere to minimise ZnO loss has been shown to be detrimental to Q.[13] As a result of these competing factors, annealing should be carried out in air in such a way as to induce order but minimise ZnO loss. Therefore, BZT–SGT samples were annealed at 1275 °C for 24h (1 day) and 168 h (1 week), respectively, following sintering at 1525 °C/2 h. Annealing for 168 h is clearly not commercially viable but ~24 h is a realistic production possibility. Table 1 presents the microwave data obtained from commercial resonators in the as-sintered, 24 h and 168 h (1 week) annealed conditions. All samples irrespective of heat treatment gave $\varepsilon_r = 29$ and $\tau_f = 0$, consistent with other authors.[2,3] However, Q increases dramatically from 54,000 at 2 GHz in the as-sintered condition to ~78,000 after 24 h at 1275 °C. After 168h at 1275 °C, Q remained high but did not increase. In this study, the Q^*f_o values of commercial BZT–SGT pucks in the as-sintered condition (108,000 GHz) are equivalent to those reported by Kageyama[2] on the BZT–SGT system. This is particularly significant when considering that the initial work by Kageyama[2] was performed on laboratory samples, typically 1 cm diameter. In the current study, universal mobile telecommunications systems (UMTS) standard pucks are investigated which are much larger with a cylindrical shape (outer and inner diameters of 27 and 10.4 mm, respectively). In general, scaling up from laboratory to production results in a drop in Q^*f_o due to a greater chance of flaws in the larger production pieces [15]. Q^*f_o of samples annealed for 24 and 168 h at 1275 °C (156,000 GHz) are greater than those reported by Kageyama[2] and, to the authors knowledge, the highest reported values for production BZT-based resonator pucks. To investigate the effect of annealing on the global structure, X-ray and neutron diffraction experiments were performed on the as-sintered and annealed samples.

Fig. 5 shows the high resolution X-ray profiles obtained from samples (a) annealed at 1275 °C/24 h, (b) 1275 °C/168 h and (c) as sintered 1525 °C/2 h. As discussed previously, 1525 °C is close to but above the order-disorder phase transition temperature for the system and Fig. 5(c) shows weak, broad intensity in the position associated with superstructure reflections. The as-sintered sample is not quenched and therefore some ordering has occurred during cooling in the furnace. In contrast, Fig. 5 (a) and (b) show discrete peaks consistent with the presence of 1:2 ordering. The relative intensities of the superstructure $\pm^1/_3\{hkl\}$ reflections

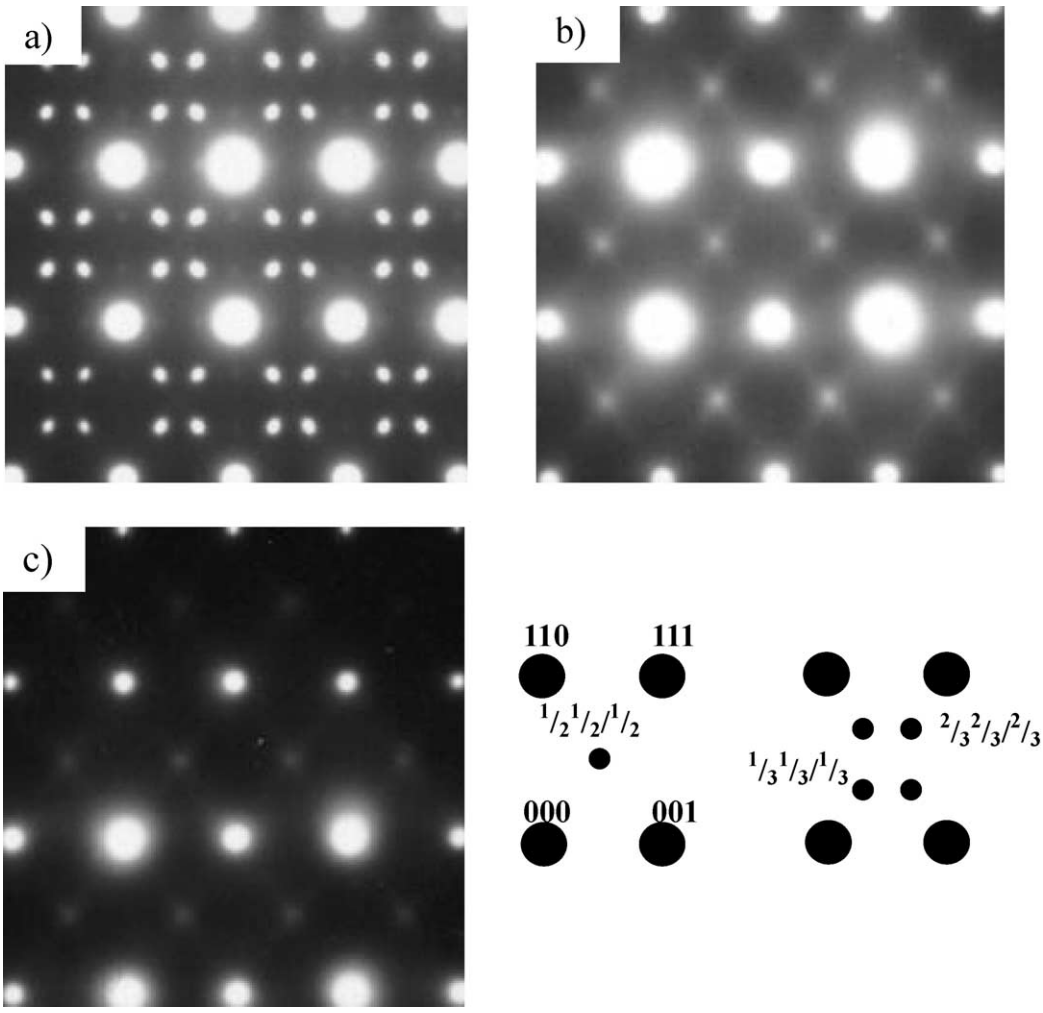

Fig. 3. <110> pseudocubic, zone axis electron diffraction patterns from samples quenched from (a) 1450 °C, (b) 1500 °C and (c) 1550 °C for 16 h. The relevant region of reciprocal space is also shown.

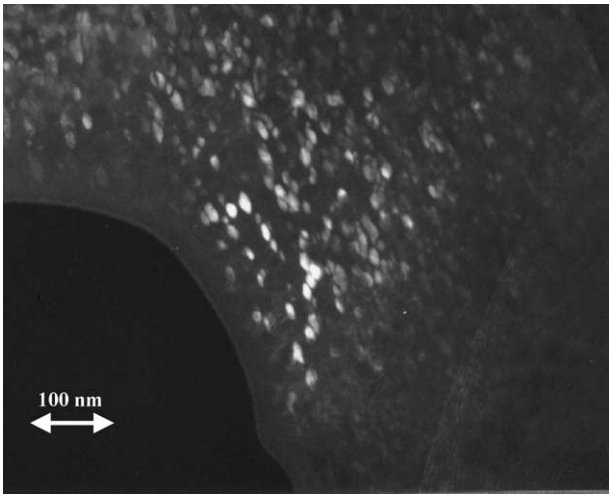

Fig. 4. Dark field TEM image obtained using a $\pm^1/_3\{hkl\}$ superlattice reflection from a grain in a sample quenched from at 1450 °C. Discrete ordered (light) regions approximately 10 nm diameter are observed.

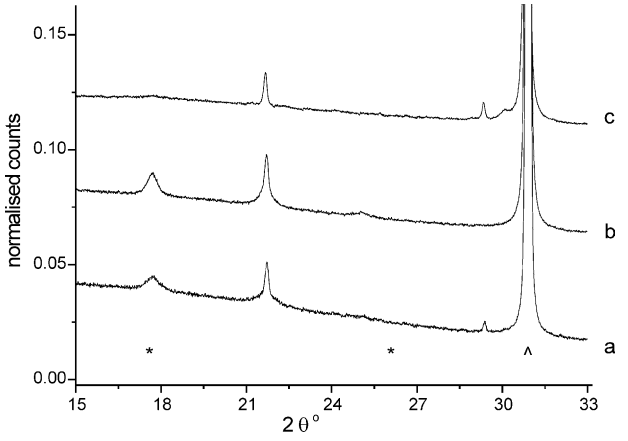

Fig. 5. Low angle XRD patterns of samples annealed at (a) 1275 °C/24 h, (b) 1275 °C/168 h and sintered at (c) as sintered (1525 °C/2 h). (∗) indicates superlattice reflections from the trigonal 1:2 ordered cell and (∧) impurity peak from $Ba_8ZnTa_6O_{24}$.

and the derived trigonal ordered domain sizes are given in Table 1.

The enhanced superstructure reflection intensities indicate the extent of 1:2 cation order coherent over the X-ray length scale increases significantly with the first 24 h anneal at 1275 °C to a level shown by quantitative Rietveld analysis to be complete. The subsequent 168 h anneal below the order–disorder temperature does not change the order parameter, but produces a significant enhancement in the X-ray averaged ordered domain size.

Detailed structural analysis and investigation of the volume-averaged structural parameters of the 24 h annealed samples was carried out using high resolution neutron powder diffraction data. Refined parameters from the neutron diffraction analysis of two nominally identical samples annealed at 1275 °C for 24 h are given in Table 2 and the resulting bond lengths and angles presented in Table 3. The data indicate the presence of small ordered domains of the 2:1 trigonal structure [98(20) Å and 126(23) Å] in both samples. It is not possible to determine directly cation temperature factors and the site distribution of dopant cations in the sample using a single histogram of data, as at least three distinct cations can occupy each octahedral B-site. (Multi-histogram refinements using resonant scattering synchrotron radiation data are required for such studies.) Accordingly, temperature factors for the cations were fixed to values determined for pure BZT[16] and cation site occupancies were refined to account for doping of Sr and Ga in the sample. This effectively allows for the change in neutron scattering length for each cation site although it should be noted that the final site occupancy values have no true physical meaning. (This method also applies to the X-ray analysis with the exception that the temperature factors for the cations were initi-

Table 2
Refined parameters from Rietveld refinement of high resolution neutron powder diffraction data on two BZT–SGT samples (denoted S1 and S2) annealed at 1275 °C for 24 h

Sample S1
Space group: $P\bar{3}m1$ (no. 164)
Lattice constants:
Phase 1 $a = 5.7812(7)$ Å, $c = 7.0823(2)$ Å, $V_c = 204.99$ Å^3; 92.7(5)% $c/a = 1.2251(2)$
Phase 2 $a = 5.7760(15)$ Å, $c = 7.1036(3)$ Å, $V_c = 205.22$ Å^3; 7.0(5)% $c/a = 1.2298(9)$
[Impurity phase: $a = 5.818(8)$ Å, $c = 19.032(4)$ Å, 0.3(5)%]
Ordered domain size $p_{(100)} = 126(23)$ Å

Atom	Site symm.	x/a	y/b	z/c	B	Site occ.
Ba(1)	1a ($\bar{3}$m.)	0.00000	0.00000	0.00000	0.51	0.98(2)
Ba(2)	2d (3m.)	0.33333	0.66667	0.6700(5)	0.51	0.99(2)
Ta	2d (3m.)	0.33333	0.66667	0.1656(5)	0.38	0.97(1)
Zn	1b ($\bar{3}$m.)	0.00000	0.00000	0.50000	0.38	1.07(2)
O(1)	6i (.m.)	0.1695(4)	−0.1695(4)	0.3353(4)	0.79(6)	1.0
O(2)	3e (.2/m.)	0.50000	0.00000	0.00000	0.95(13)	1.0

$R_p = 8.48\%$, $R_{wp} = 9.21\%$, $R_e = 3.40\%$, $\chi^2 = 7.33$ for 6610 observations and 34 variables.
($\chi^2 = 9.92$ for 6610 observations and 29 variables for single BZT phase model.)

Sample S2
Space group: $P\bar{3}m1$ (No. 164)
Lattice constants:
$a = 5.7811(2)$ Å, $c = 7.0835(4)$ Å, $V_c = 205.02$ Å^3; 92.5(3)% $c/a = 1.2253(1)$
$a = 5.782(6)$ Å, $c = 7.1193(9)$ Å, $V_c = 206.10$ Å^3; 7.4(3)% $c/a = 1.231(1)$
(Impurity phase: $a = 5.818(8)$ Å, $c = 19.034(4)$ Å, 0.1(3)%)
Domain size $p_{(100)} = 98(20)$ Å

Atom	Site symm.	x/a	y/b	z/c	B	Site occ.
Ba(1)	1a ($\bar{3}$m.)	0.00000	0.00000	0.00000	0.51	0.98(2)
Ba(2)	2d (3m.)	0.33333	0.66667	0.6700(5)	0.51	0.99(2)
Ta	2d (3m.)	0.33333	0.66667	0.1656(5)	0.38	0.97(1)
Zn	1b ($\bar{3}$m.)	0.00000	0.00000	0.50000	0.38	1.07(2)
O(1)	6i (.m.)	0.1684(5)	−0.1684(5)	0.3331(6)	0.63(6)	1.0
O(2)	3e (.2/m.)	0.50000	0.00000	0.00000	1.10(14)	1.0

$R_p = 8.35\%$, $R_{wp} = 9.24\%$, $R_e = 2.89\%$, $\chi^2 = 10.00$ for 6610 observations and 34 variables.
($\chi^2 = 14.88$ for 6610 observations and 29 variables for single BZT phase model.)

Table 3
Bond lengths (Å) and angles (°) for samples S1 and S2 of BZT–SGT annealed at 1275 °C for 24 h

S1 distances and angles					
×6	Ba(1)–O(1)	2.919(3)	×3	O(1)–Ba(1)–O(1)	180.00(18)
×6	Ba(1)–O(2)	2.891(3)	×12	O(1)–Ba(1)–O(2)	90.00(6)
×3	Ba(2)–O(1)	2.883(3)	×3	O(2)–Ba(1)–O(2)	180.00
×6	Ba(2)–O(1)	2.891(3)	×6	O(1)–Ba(2)–O(1)	89.07(11)
×3	Ba(2)–O(2)	2.872(3)	×3	O(1)–Ba(2)–O(1)	178.14(12)
			×3	O(1)–Ba(2)–O(2)	179.15(12)
			×6	O(1)–Ba(2)–O(2)	90.93(11)
×3	Ta–O(1)	2.034(4)	×3	O(1)–Ta–O(1)	88.63(17)
×3	Ta–O(2)	2.040(2)	×3	O(1)–Ta–O(2)	178.86(18)
			×6	O(1)–Ta–O(2)	90.56(10)
			×3	O(2)–Ta–O(2)	90.24(12)
×6	Zn–O(1)	2.060(4)	×6	O(1)–Zn–O(1)	91.07(12)
			×3	O(1)–Zn–O(1)	180.00(11)
			×6	O(1)–Zn–O(1)	88.93(12)
S2 distances and angles					
×6	Ba(1)–O(1)	2.900(3)	×3	O(1)–Ba(1)–O(1)	180.00(18)
×6	Ba(1)–O(2)	2.891(3)	×12	O(1)–Ba(1)–O(2)	90.00(6)
×3	Ba(2)–O(1)	2.902(3)	×3	O(2)–Ba(1)–O(2)	180.00
×6	Ba(2)–O(1)	2.891(3)	×6	O(1)–Ba(2)–O(1)	89.45(11)
×3	Ba(2)–O(2)	2.872(3)	×3	O(1)–Ba(2)–O(1)	178.89(12)
			×3	O(1)–Ba(2)–O(2)	179.16(12)
			×6	O(1)–Ba(2)–O(2)	90.55(11)
×3	Ta–O(1)	2.034(4)	×3	O(1)–Ta–O(1)	89.39(17)
×3	Ta–O(2)	2.040(2)	×3	O(1)–Ta–O(2)	179.39(18)
			×6	O(1)–Ta–O(2)	90.18(10)
			×3	O(2)–Ta–O(2)	90.25(12)
×6	Zn–O(1)	2.059(4)	×6	O(1)–Zn–O(1)	90.33(12)
			×3	O(1)–Zn–O(1)	180.00(11)
			×6	O(1)–Zn–O(1)	89.67(12)

ally refined). The two samples annealed for 24 h at 1275 °C were refined in the same manner. In both cases, the profile refinements are slightly but significantly improved (χ^2 falls from 14.0 to 10.0; it should be noted that the data are of exceptional statistical quality) by the inclusion of approximately 7% of a second trigonal BZT–SGT perovskite phase whose structural parameters were constrained to be the same as those of the majority phase but with subtly different cell parameters, as indicated in Table 2. It was not possible to refine separate and unconstrained structural parameters for each phase, and hence the refined structures are averages over both phases present. The trigonal distortion due to the cation ordering is evidenced by the deviation of the trigonal c/a ratio from the ideal cubic value of $\sqrt{(3/2)} = 1.224745$, with the minority phase in both samples having a larger trigonal distortion. This indicates that the need for two phases to model the high resolution neutron powder diffraction data is due to heterogeneity in the cation ordering throughout the sample.

The excellent reproducibility in the structural details between the two 24 h annealed samples is an important verification of the reliability of the processing sequence in generating ceramics with well-defined long-range averaged structures; the extremely good agreement in phase fractions and c/a ratios of the two BZT phases is strong evidence that this is an intrinsic feature of the BZT–SGT system under the processing conditions which produce high Q.

There is evidence from both X-ray and neutron diffraction for a distinct non-perovskite impurity phase $Ba_8ZnTa_6O_{24}$ identified from its characteristic reflection at 29.5°2θ in the X-ray patterns of Fig. 5. This data confirms the SEM observations in Fig. 1 in which laths of a ZnO deficient second phase are present on the surfaces of as-sintered and annealed samples. The high-resolution neutron data are also consistent with the presence of an unidentified second, more minor, impurity phase. Desu and O'Bryan[6] proposed the following mechanism to explain the formation of ZnO deficient phases:

$$Ba_3(ZnTa_2)O_9 \rightarrow Ba_3Ta_2O_8 + ZnO\uparrow.$$

$Ba_3Ta_2O_8$ was not observed in the current investigation. It should be noted that the identification of the impurity may only be tentative as few extra Bragg peaks are observed.

High resolution powder neutron diffraction data from the sample annealed for 168 h can only be refined satisfactorily using two BZT phases—the fits in Fig. 6 show a systematic deficiency (indicating that anisotropic strain is not responsible) on the leading edge of each Bragg reflection in the single phase fit (a), which is rectified in fit by (b) using two BZT phases. Fig. 6c and d show the effect in detail for the (2 2 0/2 0−4) reflection. The second trigonal BZT phase fraction has now increased to 20%—refined parameters from X-ray diffraction in Table 4 and high resolution neutron diffraction are given in Table 5. The bond lengths and angles derived from the neutron diffraction analysis are given in Table 6. Fig. 7 shows the fit to the X-ray powder diffraction data in which the sub and supercell reflections have been separated into separate histograms in order to allow individual peakshape functions to fit the broader $\pm {}^1/_3\{hkl\}$ reflections from the smaller cation ordered domains. The domain size monitored by neutron diffraction has increased markedly to 172(16) Å but is still smaller than those determined by X-ray. This can be assigned to the enhanced penetration depth of neutrons which sample potentially less well ordered grain interiors (ordering is characteristically greater at the grain boundary)[10] to a greater extent than the less penetrating X-rays (a 1 cm deep sample would display full (88%) transmission for neutrons but is only penetrated to a depth of 3 μm by X-rays). The difference in metal–oxygen bond length between the two symmetry inequivalent (Zn and Ta) cation sites should respond sensitively to any changes in the extent of cation order between the two sites. This difference of 0.024 Å is constant within error when comparing the samples annealed at 1275 °C for 24 h with those annealed for 168 h, and smaller than predicted from the ionic radius difference of 0.1 Å in six coordination. Recent results on pure BZT[16] indicate that well-ordered material with 60 nm domains should have mean Ta-O and Zn-O distances of 2.01 and 2.12 Å respectively contrasting with the smaller refined differences here. The off-centered environment of the Ta cation, which typically adopts three short and three long bonds, is also less distorted than expected, particularly for the samples annealed for 24 h. This reflects the limitations in the refined model of using a single set of structural parameters to model both the grain surface and the less well-ordered interior and thus reducing the differentiation between the two cation sites in the neutron-derived bond lengths. The X-ray powder diffraction data, which probe the surface regions only, are consistent with essentially complete Zn/Ta order in the 168 h annealed sample (Table 4, Fig. 7). The most pronounced effect of the extended annealing and resulting growth in the size of the cation-ordered domains on the average structure determined by neutron diffraction is seen in the marked change in the regularity of the octahedral environment at the Ta site, where the internal angles deviate much more strongly from 90 and 180° than they do in the 24 h annealed samples. Correlated with the observation of the distorted octahedral angles, the root mean square deviation of the two symmetry-inequivalent Ta–O bond lengths from the mean increases by an order of magnitude from 0.0012 Å in the 24 h annealed samples to

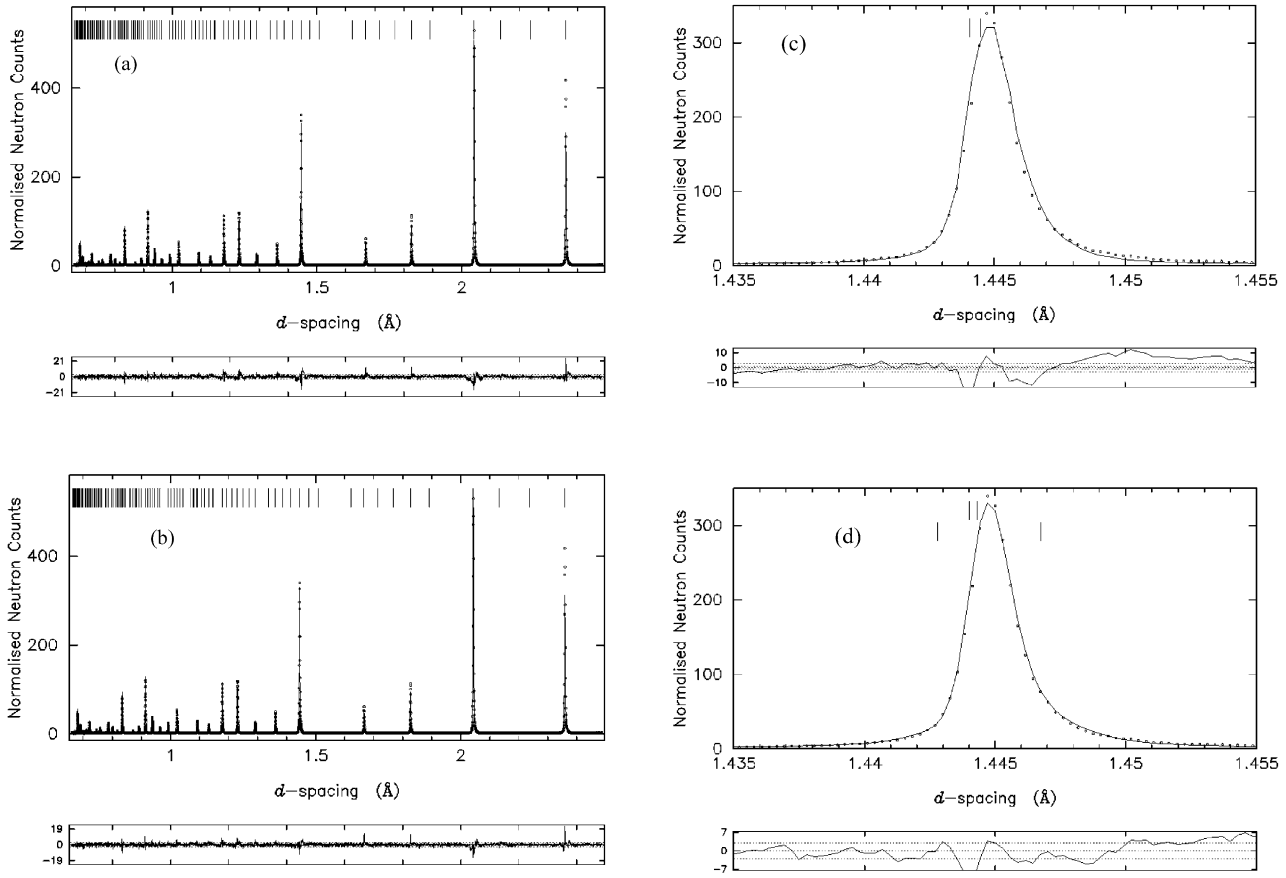

Fig. 6. (a) Rietveld profile refinement of time-of-flight powder neutron diffraction data from a sample annealed at 1275 °C for 168 h using a single phase model. Ticks mark the location of the Bragg reflections, the observed data are shown as points, the calculated fit from the model is shown as the solid line and the difference at each point divided by the esd of the point is plotted below. (b) Rietveld profile refinement of the same data shown in (a) using a model with two BZT phases. (c) An enlargement of the single-phase fit showing a representative single peak (fully overlapped 2 2 0/2 0−4 reflections) highlighting deficiencies in the fit which are particularly marked in the peak tails. (It should be noted that more marked discrepancies are observed elsewhere in the pattern when fitted as a single phase but in regions that cannot be considered as single isolated peaks.) (d) The same region as in (c) shown with the two phase model, where the improved fit, particularly to the tails of the reflection, is evident. It is this improvement across the entire profile which makes the two-phase model clearly correct. This effect is only visible with high-resolution data, and the time-of-flight technique is particularly appropriate to demonstrate it as the resolution is constant across the pattern.

Table 4
Refined parameters from Rietveld refinement of X-ray powder diffraction data on BZT–SGT annealed at 1275 °C for 168 h

S1 distances and angles
Sample: annealed at 1275 °C/168 h
Space group: $P\bar{3}m1$ (No. 164)
Lattice constants: $a = 5.7811(1)$Å $c = 7.0822(2)$Å V = 204.986(1)Å^3 $c/a = 1.22506(3)$

Atom	Site symm.	x/a	y/b	z/c	100 U_{iso} (Å^2)	Site occ.
Ba	1a ($\bar{3}$m.)	0	0	0	0.77(4)	0.96(1)
Ba	2d (3m.)	1/3	2/3	0.6646(5)	0.77(4)	0.994(9)
Ta	2d (3m.)	1/3	2/3	0.1690(4)	0.11(3)	0.926(8)
Zn	1b ($\bar{3}$m.)	0	0	1/2	0.11(3)	1.07(1)
O1	6i (.m.)	0.166(1)	−0.166(1)	0.352(2)	0.250	1
O2	3e (.2/m.)	0.5	0	0	0.250	1

R-factors—Histogram 1(subcell reflections only) R_p 4.40 R_{wp} 5.74;
Histogram 2 (supercell reflections only) R_p 2.64 R_{wp} 3.44;
Totals R_p 3.67 R_{wp} 4.91;
χ^2 2.889 for seven variables in final cycle.

Table 5
Refined parameters from Rietveld refinement of high resolution neutron powder diffraction data on BZT–SGT annealed at 1275 °C for 168 h

Sample: annealed at 1275 °C/168 h
Space group: $P\bar{3}m1$ (No. 164)
Lattice constants:
Phase 1 $a = 5.7811(8)$ Å, $c = 7.0823(2)$ Å, $V_c = 204.98$ Å^3; 80.4(5)%
$c/a = 1.2251(2)$
Phase 2 $a = 5.7760(15)$ Å, $c = 7.1036(3)$ Å, $V_c = 205.22$ Å^3; 19.6(5)%
$c/a = 1.2298(3)$
Domain size $p_{(100)} = 172(16)$ Å

Atom	Site symm.	x/a	y/b	z/c	B	Site occ.
Ba(1)	1a ($\bar{3}$m.)	0.00000	0.00000	0.00000	0.51	1.00(2)
Ba(2)	2d (3m.)	0.33333	0.66667	0.6682(5)	0.51	0.95(2)
Ta	2d (3m.)	0.33333	0.66667	0.1575(5)	0.38	0.95(1)
Zn	1b ($\bar{3}$m.)	0.00000	0.00000	0.50000	0.38	1.09(2)
O(1)	6i (.m.)	0.1687(4)	−0.1687(4)	0.3356(4)	0.98(5)	1.0
O(2)	3e (.2/m.)	0.50000	0.00000	0.00000	0.99(8)	1.0

$R_p = 8.84\%$, $R_{wp} = 9.91\%$, $R_e = 3.12\%$, $\chi^2 = 10.07$ for 6610 observations and 30 variables.
($\chi^2 = 14.95$ for 6610 observations and 25 variables for single phase model.)

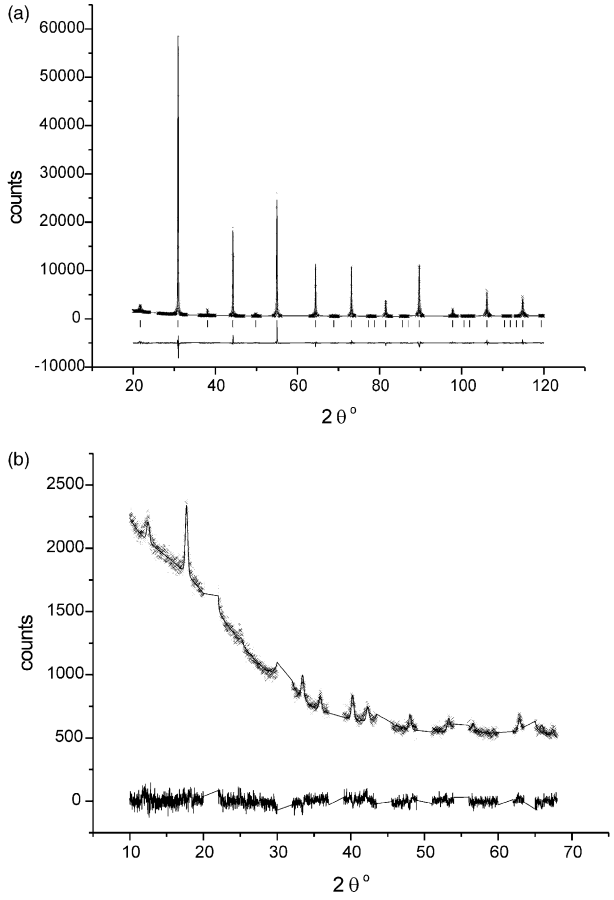

Fig. 7. Observed (crosses), calculated (solid line) and difference profiles of sample annealed at 1275 °C for 168 h. Reflection markers are indicated by tick marks. (a) Subcell reflections only, (b) supercell reflections, fit using a second peakshape function to allow their enhanced width to be fit satisfactorily.

Table 6
Bond lengths (Å) and angles (°) for BZT–SGT annealed at 1275 °C for 168 h derived from neutron powder diffraction data

×6	Ba(1)–O(1)	2.917(3)	×3	O(1)–Ba(1)–O(1)	180.00(18)
×6	Ba(1)–O(2)	2.891(3)	×12	O(1)–Ba(1)–O(2)	90.00(6)
×3	Ba(2)–O(1)	2.874(3)	×3	O(2)–Ba(1)–O(2)	180.00
×6	Ba(2)–O(1)	2.891(3)	×6	O(1)–Ba(2)–O(1)	89.33(11)
×3	Ba(2)–O(2)	2.883(3)	×3	O(1)–Ba(2)–O(1)	178.67(12)
			×3	O(1)–Ba(2)–O(2)	179.62(12)
			×6	O(1)–Ba(2)–O(2)	90.67(11)
×3	Ta–O(1)	2.076(4)	×3	O(1)–Ta–O(1)	86.88(17)
×3	Ta–O(2)	2.007(2)	×3	O(1)–Ta–O(2)	176.31(18)
			×6	O(1)–Ta–O(2)	90.44(10)
			×3	O(2)–Ta–O(2)	92.12(12)
×6	Zn–O(1)	2.052(4)	×6	O(1)–Zn–O(1)	90.99(12)
			×3	O(1)–Zn–O(1)	180.00(11)
			×6	O(1)–Zn–O(1)	89.01(12)

0.0141 Å in the 168 h annealed sample (Fig. 8). These diffraction-determined bond lengths and angles are averages over the diffraction length scale of several hundred angstroms, but the absence of a drastic enhancement in the oxide displacement parameters compared with the 24 h annealed samples indicates that there is no disordered contribution to these changes incoherent with the $P\bar{3}m1$ space group symmetry.

The signature of cation ordering over the X-ray diffraction length scale of $\geqslant 100$ Å in BZT derivatives is the observation of superstructure reflections—the associated trigonal splitting of the fundamental cubic reflections reflects the effect of the symmetry lowering on the subcell in a manner that is coherent across the cation-ordered domain (both antiphase and orientational) boundaries. The integrated intensities of the superstructure reflections do not increase significantly on extended annealing at 1275 °C, which suggests that the extent of order within the domains does not increase on this timescale despite the increase in the domain size. The absence of a pronounced effect of the extended annealing on Q beyond the dramatic increase observed in the first 24 hours suggests that it is the formation of the short coherence length, long-range ordered domains upon the first anneal below the order–disorder temperature which controls Q; further enhancement of the extent of these domains or the amount of ordering at the grain boundaries does not make a significant difference.

Although enhanced ordered domain size on the neutron diffraction length scale does not enhance Q, it does allow the neutron probe to define exactly the local structural requirements for the high Q by allowing the ordered structure to extend over a sufficient distance that the true bond lengths at both metal sites can be determined by diffraction. The d^0 cations of the early transition metals often display reduced regularity of their coordination environment as a pronounced feature

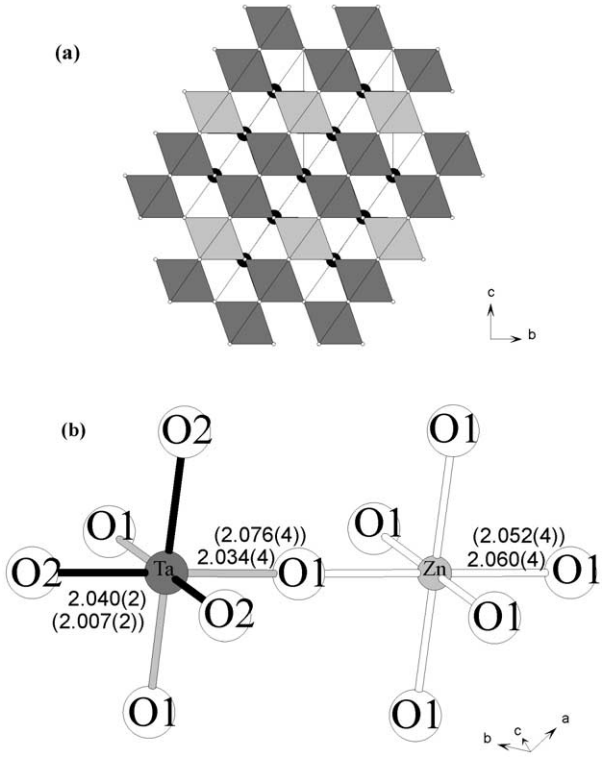

Fig. 8. (a) The 2:1 ordered structure of BZT viewed perpendicular to the stacking direction of the cation ordered octahedral layers. Zn octahedra are shaded light grey. (b) The cation ordering shown in (a) produces a Ta site that is non-centrosymmetric, with two distinct bond lengths marked as black and light grey. The difference between these two symmetry-inequivalent bonds as measured in the average structure determined by neutron powder diffraction increases on annealing for 24–168 h (bond lengths for the 168 h structure are shown in parentheses, those for the 24 h structure without). Bond lengths at the neighbouring Zn site are also shown.

of their structural chemistry, and enhanced ordering of Zn and Ta would be expected to drive displacements of the oxide anions to produce a much less regular environment at the d^0 Ta(V) than the d^{10} Zn(II) site. The true local structure within the smaller cation-ordered domains of the 24 h annealed sample may display similar distortions at the metal sites at the centres of the domains, but a greater fraction of the cations will be located in or near domain boundaries where faulting in the strict layered cation alternation will reduce the volume-averaged distinction between the two sites, as reflected in the refined neutron parameters. Once the 2:1 cation ordering has developed sufficiently to allow development of the appropriate asymmetric coordination at sufficient Ta(V) sites, growth in the size of the ordered domains beyond that established in the first 1275 °C anneal has a less significant effect on Q. This may explain the dramatic effect of the first anneal at 1275 °C and the less pronounced effect of further domain growth once the domains are large enough to allow the long-range correlation of the distorted TaO_6 environment to develop.

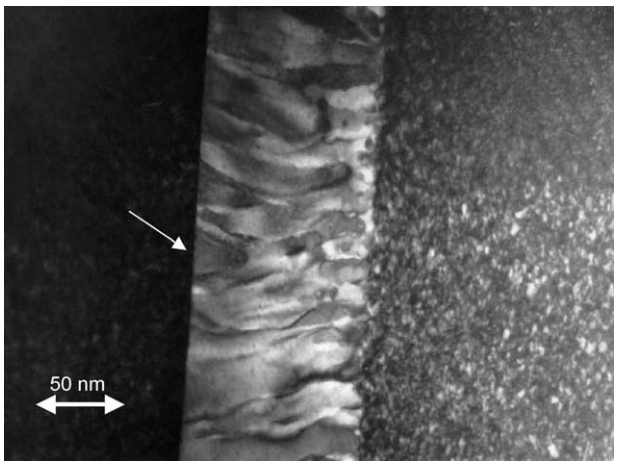

Fig. 9. Dark field TEM image obtained using $\pm{}^1/_3\{hkl\}$ ordered superlattice reflections from BZT–SGT annealed at 1275 °C/168 h. The bright central band is a region of complete order containing APBs at one side of the grain boundary (arrowed). Small ordered regions are visible in strong contrast on the right hand side but are out of contrast on the left hand side of the image.

In order to investigate further the ordering of BZT–SGT and, in particular, the domain size and distribution within individual grains TEM was performed. Fig. 9 shows dark field TEM images obtained using ordered superlattice reflections from BZT–SGT annealed at 1275 °C for 168 h. On the right hand side of the image, small ordered regions (10–20 nm) are observed which give rise to electron diffraction patterns which demonstrate the existence of two orientational domain variants, Fig. 10a. On the left hand side of Fig. 9, a large ordered concentric shell (~125 nm wide) immediately adjacent to the grain boundary is observed. The concentric shell is formed from a single ordered variant with Zn^{2+} and Ta^{5+} occupying only one set of {111} planes [e.g. (111)], as illustrated by the electron diffraction pattern in Fig. 10b. Other grains showed similar ordered shells that typically were all 100–200 nm wide. Similar dark field images and electron diffraction patterns were obtained from samples annealed for 24 h at 1275 °C. In addition, planar defects are observed running approximately perpendicular to the grain boundary. Their ribbon-like contrast and sensitivity to dark field superlattice imaging define them as translational domain walls, commonly referred to as APBs. In contrast, as-sintered ceramics show evidence of short-range order, identical to that observed in samples quenched from 1500 °C and 1550 °C, Fig. 3b and c.

TEM clearly confirms the presence in the microstructure of two distinct ordered phases in BZT–SGT annealed for 1275 °C for 24 and 168 h. The domain sizes refined by neutron and X-ray diffraction fit well to those observed by TEM in the grain core (~10–20 nm) but the grain shell is typically 100–200 nm wide and does not match the domain size calculated from neutron data. However, the APBs in the shell are at a spacing of

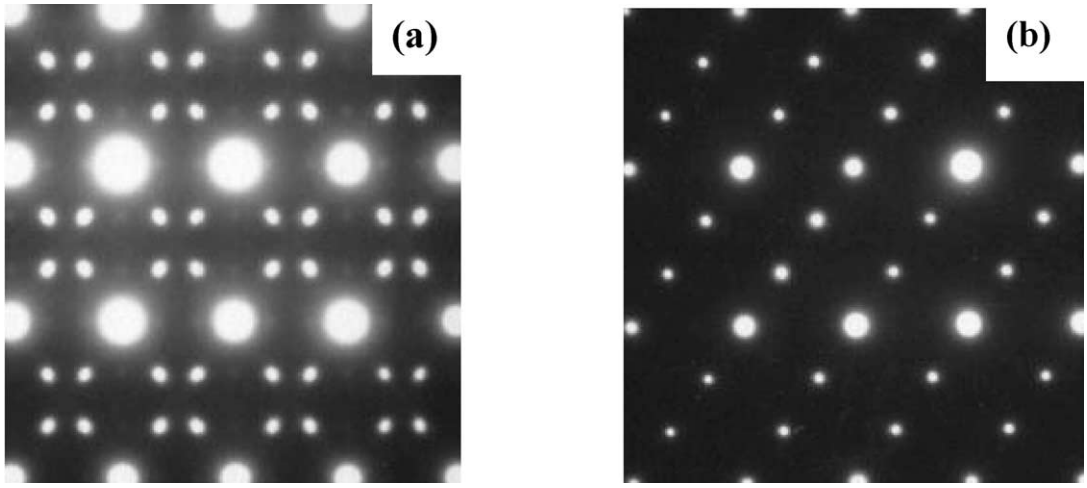

Fig. 10. <110> pseudocubic zone axis electron diffraction patterns from a sample annealed at 1275 °C/168 h obtained from (a) grain exterior (shell) and (b) the grain interior (core).

approximately every 20–30 nm. This reduces the effective neutron and X-ray diffracting volume to that of the distance between defects which is more consistent with the calculated domain sizes. Moreover, TEM indicates that the ordered shells only appear on one side of the grain boundary and are therefore present in every second grain. Given the above information and assuming an average grain diameter of ~5 μm, the volume fraction of ordered shell may be estimated from the TEM data,

$$\text{Volume fraction ordered shell} = \frac{\text{Volume of grain} - \text{volume of core region}}{2 \times \text{Volume of grain}}.$$

Therefore,

$$\text{Volume fraction ordered shell} = \frac{4/3\pi r^3 - 4/3\pi(r-0.2)^3}{2 \times 4/3\pi r^3}$$

$$\text{Volume fraction of ordered shell} = 0.11 = 11\%$$

where r is the radius of a grain (~2.5 μm) and assuming an upper limit of 0.2 μm for the width of the ordered shell.

The volume fractions of larger domain trigonal BZT estimated by neutron diffraction for the 24 and 168 h annealed samples are 7 and 20%, respectively. Eleven per cent volume fraction of ordered shell estimated from TEM data is in good agreement with these two figures. It should be noted that TEM is only able to observe the local microstructure and grain and ordered shell sizes refer to analyses from no more than 100–200 grains of the 1275 °C/168 h sample. It is only assumed that the grain and shell size remain constant across the sample. Neutron diffraction confirms however, that two distinct

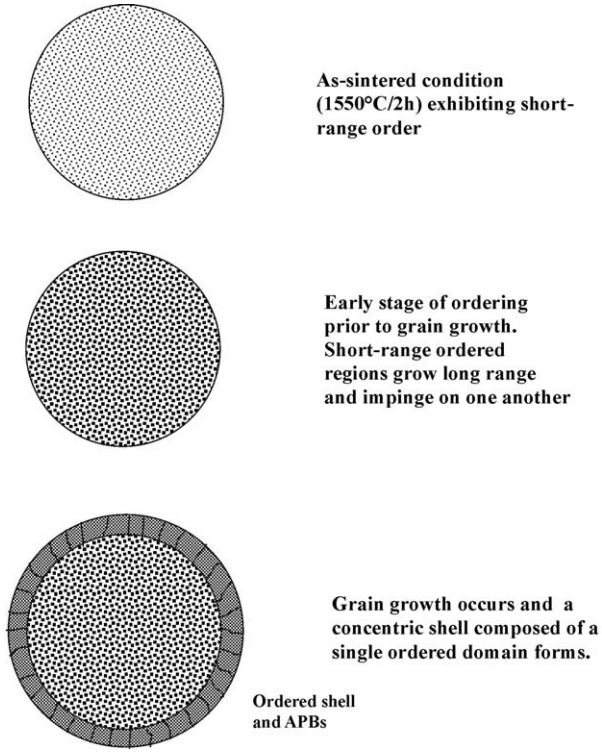

Fig. 11. Schematic illustrating the ordering mechanism in BZT–SGT.

2:1 ordered BZT phases are present globally throughout annealed pucks and unequivocally differentiates between samples heat treated at 1275 °C for 24 and 168 h (7 and 20% of second BZT phase, respectively). Furthermore, X-ray integrated intensities indicate that the extent of order increases significantly upon annealing at 1275 °C for 24 h but is constant with further treatment at this temperature. TEM is statistically unable to perform these latter functions without the fabrication of a large number of thin foils.

The above observations reconcile the properties of the resonators observed both locally (TEM) and integrated over the entire sample (due to the penetrating power of the neutrons). Detailed refinement of the metal site occupancies in both phases would reveal whether dopant segregation or ZnO loss was important in driving this enhanced ordering, but would require several histograms of anomalous X-ray scattering data at absorption edges of each of the elements involved.

From a combination of dark field imaging, X-ray, neutron and electron diffraction observations, an ordering mechanism may be deduced for high Q samples annealed at 1275 °C. Initially ordering occurs homogeneously throughout the sample by the nucleation of small ordered domains. The nucleation density is high due to preexisting short range ordered regions in the as-sintered ceramic. These domains grow from ~10 to 20 nm in size at which stage they impinge their neighbours, forming either translational (APBs), orientational or mixed domain walls.[9] Where orientational or mixed domains impinge, a strained interface develops which gives rise to a mottled bright field contrast reported by many authors.[7–9] During extended heat treatment however, slight grain growth occurs with the formation of an ordered BZT–SGT shell containing elongated APB's. Since grains grow at the expense of their neighbours, concentric ordered shells are present in alternate but not all crystallites. This effect has been observed for order–disorder behaviour in metallic systems such as Ni_2V[17] in which elongated APBs at grain exteriors were attributed to grain boundary migration. This mechanism is schematically illustrated in Fig. 11.

4. Conclusions

1. The order–disorder transition for BZT–SGT occurs at approximately 1500 °C.
2. Annealing a UMTS specification puck for 24 h at 1275 °C results in an increase in Q^*f_o from 108,000 GHz (as sintered) to 156,000 GHz (annealed). Further annealing does not improve Q.
3. The increase in Q is commensurate with an increase in the degree of order. A two phase BZT microstructure develops composed of grains with concentric ordered shells (100 nm) of BZT around a core containing smaller ordered domains (~10–20 nm). This occurs throughout the entire resonator as shown by the need to use two BZT phases to obtain a satisfactory refinement of neutron diffraction data collected on samples after extended anneals.
4. The enhanced cation ordering on annealing below the order–disorder temperature allows long range co-operative distortion of the TaO_6 octahedra, resulting in the correct coordination environment for a d^0 transition metal. This effect produces the enhancement of Q at 1275 °C/24 h. Further annealing does not improve Q as the Ta cations have already adopted their appropriate and commonly observed coordination environment; the enhanced domain size resulting from the annealing does however allow this environment to be probed directly by neutron diffraction.
5. A ZnO deficient $Ba_8ZnTa_6O_{24}$ phase, rather than $Ba_3Ta_2O_8$ was present particularly on the surface of all samples.

Acknowledgements

Dr. Reaney would like to thank Dr. P. Korgul and Ms. D. Bussey for their continued support with electron microscopy.

References

1. Tamura, H., Konoike, T., Sakabe, Y. and Wakino, K., Improved high-Q dielectric resonator with complex perovskite structure. *J. Am. Ceram. Soc.*, 1984, **67**, C59–C61.
2. Kageyama, K., Crystal structure and microwave dielectric properties of $Ba(Zn_{1/3}Ta_{2/3})O_3$–$(Sr,Ba)(Ga_{1/2}Ta_{1/2})O_3$ ceramic. *J. Am. Ceram. Soc.*, 1992, **75**(7), 1767–1771.
3. Davies, P. K. and Tong, J., Effect of ordering-induced domain boundaries on low-loss $Ba(Zn_{1/3}Ta_{2/3})O_3$–$BaZrO_3$ perovskite microwave dielectrics. *J. Am. Ceram. Soc.*, 1997, **80**(7), 1727–1740.
4. Galasso, F. S., *Stucture Properties and Preparation of Perovskite Type Compounds*. Pergamon Press, Oxford, London, 1969.
5. Jacobson, A. J., Collins, B. M. and Fender, B. E. F., A powder neutron and x-ray diffraction determination of the structure of $Ba_3Ta_2ZnO_9$: an investigation of perovskite phases in the system Ba–Ta–Zn–O and the preparation of $Ba_2TaCdO_{5.5}$ and $Ba_2CeInO_{5.5}$. *Acta Cryst.*, 1976, **B32**, 1083–1087.
6. Desu, S. B. and O'Bryan, H. M., Microwave loss quality of $Ba(Zn_{1/3}Ta_{2/3})O_3$ ceramics. *J. Am. Ceram. Soc.*, 1985, **68**(10), 546–551.
7. Barber, D. J., Moulding, K. M. and Zhou, J. I., Structural order in $Ba(Zn_{1/3}Ta_{2/3})O_3$, $Ba(Zn_{1/3}Nb_{2/3})O_3$ and $Ba(Mg_{1/3}Ta_{2/3})O_3$ microwave dielectric ceramics. *J. Mater. Sci.*, 1997, **32**, 1531–1544.
8. Harmer, M. P., Chen, J., Peng, P., Chan, H. M. and Smyth, D. M., Control of microchemical ordering in relaxor ferroelectrics and related compounds. *Ferroelectrics*, 1989, **97**, 263–274.
9. Reaney, I. M., Colla, E. L. and Setter, N., Dielectric and structural characteristics of Ba- and Sr-based complex perovskites as a function of tolerance factor. *Jap. J. Appl. Phys*, 1994, **33**(7A), 3984–3990.
10. Randall, C. A., Barber, D. J., Whatmore, R. W. and Groves, P., A TEM study of ordering in the perovskite, $Pb(Sc_{1/2}Ta_{1/2})O_3$. *J. Mater. Sci.*, 1986, **21**, 4456–4462.
11. Randall, C. A., Barber, D. J. and Whatmore, R. W., In situ TEM experiments on perovskite-structured ferroelectric relaxor materials. *J. Microscopy*, 1987, **145**(3), 275–291.
12. Larson, A. C. and von Dreele, R. B., *General Structure Analysis System (GSAS)*. Los Alamos National Laboratories, 1990.
13. Kawashima, S., Influence of ZnO evaporation on microwave

dielectric loss and sinterability of $Ba(Zn_{1/3}Ta_{2/3})O_3$ ceramics. *Bull., Am. Ceram. Soc.*, 1993, **72**(5), 120–126.
14. Kawashima, S., Nishida, M., Ueda, T. and Ouchi, H., $Ba(Zn_{1/3}Ta_{2/3})O_3$ ceramics with low dielectric loss at microwave frequencies. *J. Am. Ceram. Soc.*, 1983, **66**(6), 421–423.
15. Iddles, D., Filtronics Comtek, UK, Private communication.
16. Bieringer, M., Moussa, S. M., Noailles, L. D., Ibberson, R. M., Rosseinsky, M. J. and Kiely, C. J., *Chemistry of Materials*, 2003, **15**, 586–597.
17. Tanner, L. E., *Acta. Met.*, 1972, **20**, 1197.